Title No. 114-M17

Multiaxial Expansion-Stress Relationship for Alkali Silica Reaction-Affected Concrete

by B. P. Gautam, D. K. Panesar, S. A. Sheikh, and F. J. Vecchio

Many concrete structures around the world are experiencing expansion of concrete due to alkali-silica reaction (ASR). ASR expansion is reduced in the direction of compressive stress and is transferred to the unstressed directions. However, the relationship between ASR expansion and a multiaxial stress state in concrete, which is often the case in concrete structures, is inadequately understood. This paper presents a relationship between ASR expansion and the stress state of concrete based on experimentally determined triaxial expansions of unstressed and uniaxially, biaxially, and triaxially stressed concrete cube specimens. The expansion-stress relationship is not coupled with reaction kinetics and is isolated from the effect of creep and shrinkage by subtracting the deformations measured on non-reactive control specimens. The proposed relationship was implemented in a finite element program to predict the measured expansion values on concrete cube specimens. The predicted expansions are in reasonable agreement with the measured expansions.

INTRODUCTION

Expansion due to alkali-silica reaction (ASR) has caused serious consequences in many concrete structures around the world.[1] ASR is a complicated reaction that is influenced by several factors such as temperature, humidity, alkali content of concrete, type and content of reactive aggregate, and stress state. The reaction usually lasts for many years in concrete structures. Studies on ASR over the past several decades have clarified most of the mechanisms of ASR. However, the effect of stress state on ASR expansion is not yet well understood.

Several studies have examined the influence of stress on the ASR expansion of concrete by maintaining uniaxial compressive stress in concrete that was undergoing ASR.[2-6] Such studies have revealed that expansion is reduced in the direction of compressive stress and is transferred to the unstressed directions. The phenomena of both reduction and transfer complicate the relationship between the ASR expansion and the stress state. Studies limited to uniaxial stress are inadequate for understanding the relationship between the ASR expansion that occurs volumetrically and the stress state that can be multiaxial.

Attempts have been made to experimentally investigate the effect of multiaxial stress on the ASR expansion of concrete.[7-10] To experimentally investigate the effect of multiaxial stress on ASR expansion, Gravel et al.[7] measured the triaxial expansion of a cube specimen subjected to biaxial stress. However, the study[7] brought limited understanding of the effect of multiaxial stress on ASR expansion. Multon and Toutlemonde[8] investigated the mechanism of ASR expansion when concrete is subjected to triaxial restraints. Axial stress in cylinder specimens was applied through a load cell and the lateral restraint was provided through passive confinement by steel rings. The study[8] concluded that "the ASR volumetric imposed strain can be considered as constant whatever the stress state." In contrast, the work by Gautam and Panesar[9] reported that the volumetric strains vary with stress state, in particular in the triaxially stressed condition.

Numerical studies have been performed by considering the influence of stress on ASR expansion.[11-17] However, "due to lack of sufficient experimental data," the relationship between expansion and stress had to rely on "engineering common sense."[17] Moreover, due to the incorporation of the reaction kinetics[15,17] and the creep of concrete,[15] models have become extremely complex, and several assumptions have to be made in analyzing concrete structures with such models. In essence, the models lack an experimental basis involving ASR expansion of concrete under multiaxial stress state.

An experimental investigation was performed by Gautam and Panesar[9] that measured triaxial ASR expansion in several unrestrained and restrained concrete specimens subjected to uniaxial, biaxial or triaxial stresses. The experimental results showed: (i) the reduction of ASR expansion due to stress; (ii) the transfer of ASR expansion from stressed to unstressed direction; and (iii) the reduction in volumetric expansion due to triaxial stress. These three outcomes and observations form the basis for developing a relationship between the ASR expansion and the stress state of concrete. This paper is focused on the influence of stress state on the expansion of concrete due to ASR, and a relationship is proposed. The reaction kinetics component is decoupled from the effect of stress based on experimental observations. Also, the effect of creep and shrinkage is isolated by subtracting deformation measurements on non-reactive specimens from the measurements on reactive specimens. The proposed relationship is a simple and reasonably accurate tool for the analysis of ASR-affected concrete structures.

Table 1—Average applied stress in concrete cube specimens for seven stress states

Stress state	Designation	Average applied stress, MPa (psi)			Number of reactive cube specimens	Number of control cube specimens
		f_x	f_y	f_z		
No-stress	n (0, 0, 0)	0 (0)	0 (0)	0 (0)	3	1
Uniaxial	u (3.9, 0, 0)	3.9 (566)	0 (0)	0 (0)	3	1
	U (9.6, 0, 0)	9.6 (1392)	0 (0)	0 (0)	3	1
Biaxial	b (3.9, 3.9, 0)	3.9 (566)	3.9 (566)	0 (0)	3	1
	B (9.6, 3.9, 0)	9.6 (1392)	3.9 (566)	0 (0)	3	1
Triaxial	t (3.9, 3.9, 3.9)	3.9 (566)	3.9 (566)	3.9 (566)	3	1
	T (9.6, 3.9, 3.9)	9.6 (1392)	3.9 (566)	3.9 (566)	3	1

RESEARCH SIGNIFICANCE

ASR expansion is influenced by the stress state in concrete. Various models have been proposed to relate the ASR expansion with the stress state. However, the models cannot be substantiated in the absence of an experimental investigation in a three-dimensional (3-D) stress state. This study proposes an expansion-stress relationship for ASR expansion which is rooted in an experimental study involving stresses in three directions. The relationship has been validated by comparing the experimental results with results from a numerical analysis. The relationship provides a simple and reasonably accurate basis for the numerical simulation of ASR-affected concrete structures.

EXPERIMENTAL INVESTIGATION
Concrete specimens

The experimental study involved 28 concrete cube specimens of 254 mm (10 in.) size subjected to multiaxial stresses.[9] Table 1 details the seven (compressive) stress states that include a no-stress condition, uniaxial stress, biaxial stress, and triaxial stress. Two concrete mixture designs were used: (i) a reactive concrete mixture with reactive coarse aggregate and non-reactive fine aggregate; and (ii) a non-reactive control mixture with non-reactive coarse and non-reactive fine aggregate. The concrete mixture designs were based on the proportions detailed in ASTM C1293.[18] The cement content of concrete was 420 kg/m³ (707.9 lb/yd³) and the alkali level of concrete was 5.25 kg/m³ (8.85 lb/yd³) Na_2O_{eq}. Natural sand from Orillia, ON, Canada was used as the non-reactive fine aggregate. Spratt aggregate (crushed siliceous limestone) from Stittsville, ON, Canada was used as the reactive coarse aggregate for the reactive concrete mixture. Crushed limestone from Milton, ON, Canada was used as the non-reactive coarse aggregate for the non-reactive mixture. No admixtures or supplementary cementitious materials were used. The water-cement ratio of both mixtures was 0.44.

Loading and conditioning of specimens

Stress application in the cube specimens was performed at an age of 52 to 56 days. The post-tensioning method of prestressing was used to apply and sustain the desired compressive stresses in the concrete specimens, and is detailed in Gautam and Panesar.[9] In any stressed direction, stress was applied by using four high-strength bolts with a diameter either of 12.7 or 19.0 mm (0.5 or 0.75 in.) tightened against a pair of bearing plates for each bolt. A neck was formed in each bolt by removing the threads from a 40 mm (1.6 in.) long section at the mid-length. A strain gauge was affixed at the neck and was used to monitor the strain in the bolt as a means of applying desired stress in the bolt. Reasonably constant stress state was maintained by stressing the bolts close to yielding. Any likely expansion due to ASR would yield the bolts, and the stress level in the bolt would remain reasonably constant at the yield plateau for large strains in excess of 5000 microstrain (0.5% strain). Figure 1(a) shows the arrangement of multiaxial stress application in a specimen in a 3-D view. Figures 1(b), (c), and (d) detail the YZ, XZ, and XY planes, respectively, for 3.9 MPa (566 psi) stress each in the x-, y-, and z-directions. Figure 1(b) also shows a dashed line representing the relatively larger bearing plate for 9.6 MPa (1392 psi) stress in the x-direction. The applied stress in concrete in a direction was calculated as the total compressive force imposed by four bolts divided by the cross-sectional area of concrete. Bearing plates were chosen to cover the concrete surface only partially by considering the space required for performing non-destructive tests and for ensuring exposure of concrete to moisture, and also for limiting the mass of the specimens. This caused some stress concentration effect to prevail in the specimens. The stress distribution was obtained through a numerical analysis in this study.

From the day of demolding to the age of 180 days, the specimens were cured at room temperature (23 ± 3°C [73.4 ± 5.4°F]) with frequently watered wet burlap further covered with a plastic sheet. At the age of 180 days, the specimens were subjected to accelerated curing at 50 ± 0.5°C (122 ± 0.9°F) temperature and >95% relative humidity (RH) in a purposefully built acceleration chamber as discussed by Gautam.[19]

Expansion measurement

Expansion of the cube specimens was measured in the x-, y- and z-directions. In each direction, expansion was taken as the average of four measurements which were taken on four pairs of studs embedded in concrete during casting, as shown in Fig. 1(a). For the cube specimen of 254 mm (10 in.) length, the studs were 30 mm (1.18 in.) long, thus the gauge length for the expansion measurement was 194 mm (7.64 in.).
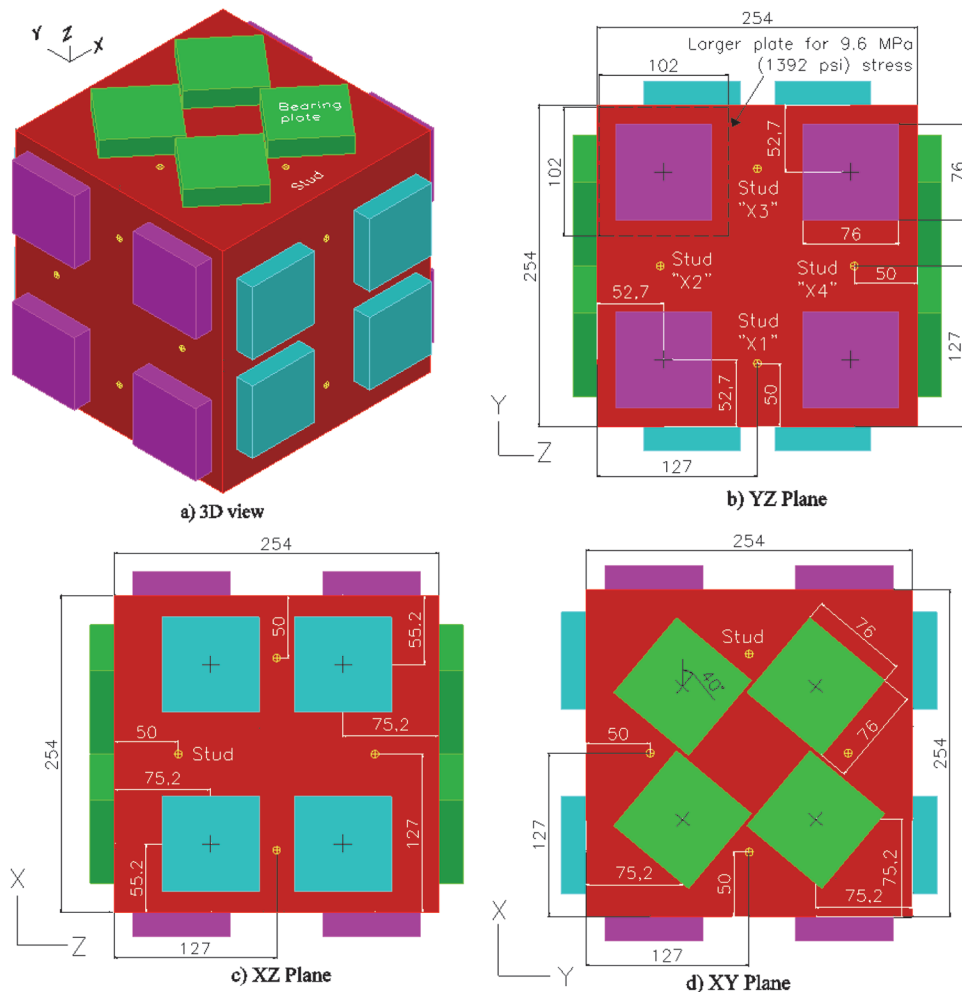
a) 3D view

b) YZ Plane

c) XZ Plane

d) XY Plane

Fig. 1—Multiaxial stress application arrangement in cube specimens and studs for expansion measurement. (Note: plates in XY plane were rotated to make space for performing nondestructive tests; dimensions are in mm; 1 mm = 0.039 in.)

Expansion was measured using a digital micrometer, with a resolution of 1 μm (0.04 mil), and a manufacturer-specified accuracy of ±4 μm (±0.16 mil). Before taking the measurements of a cube specimen, the micrometer was calibrated to the standard reference invar bar. The initial (reference) micrometer measurements were taken immediately after demolding at the age of one day.

Following the initial measurement, expansion measurements were taken at 28, 52, 57, 120, 210, 235, 270, 315, 360, 430, 485, and 545 days. As stress was applied to the specimens at the age of 52 to 56 days, the 52-day measurement served as a pre-loading measurement and the 57-day measurement served as a post-loading measurement. After subjecting the specimens to accelerated curing (50 ± 0.5°C [122 ± 0.9°F] and >95% RH) at the age of 180 days, expansion measurements were performed by taking the specimens out of the chamber and acclimatizing at room temperature for approximately 24 hours.

EXPERIMENTAL RESULTS AND ANALYSIS

Table 2 presents the axial expansions of the reactive concrete cube specimens for all stress states. It should be noted that the specimens were introduced to the accelerated curing at 50 ± 0.5°C (122 ± 0.9°F) beginning 180 days after casting. The results are the average of multiple specimens for a given stress state. Each expansion value in Table 2 is an average of three specimens up to 270 days. Between 315 and 430 days, each expansion value is an average of three specimens for the biaxially stressed specimens and of two specimens for the other specimens. Between 485 and 545 days, each expansion value represents only one cube specimen. (Table A1 in the Appendix shows the standard deviation for multiple specimens corresponding to the average measurements presented in Table 2).

The nonreactive concrete cube specimens were also measured for expansion (or contraction) at the same ages. The maximum axial expansion for the no-stress non-reactive specimen was 0.016% at 545 days. The maximum observed expansion for the non-reactive specimens was 0.037%. Only the z-direction of the B (9.6, 3.9, 0) specimen and the y- and z-directions of the U (9.6, 0, 0) specimen showed a relatively larger expansion of the nonreactive specimens in the range of 0.03 to 0.037%. This must have been contributed by the stress in the other directions. The effect of stress, other than on ASR expansion, was assumed identical for the reactive and the non-reactive specimens for a given direction for a given stress state. Moreover, the effect of creep and shrinkage (and swelling other than ASR expansion) was assumed similar for the reactive and the nonreactive specimens for a given direction for a given stress state. Therefore,

Table 2—As-measured axial expansion of reactive specimens, %

Axis	Age (days) → Stress state ↓	28	52	57	120	210	235	270	315	360	430	485	545
X	n (0, 0, 0)	−0.004	−0.005	−0.005	0.002	0.054	0.083	0.110	0.114	0.132	0.140	0.140	0.139
	u (3.9, 0, 0)	−0.001	−0.005	−0.011	−0.002	0.028	0.044	0.062	0.077	0.092	0.093	0.098	0.098
	U (9.6, 0, 0)	−0.009	−0.010	−0.028	−0.027	−0.015	−0.009	0.000	−0.003	0.004	0.004	0.008	0.009
	b (3.9, 3.9, 0)	0.000	0.001	−0.002	0.003	0.037	0.057	0.072	0.083	0.091	0.095	0.095	0.095
	B (9.6, 3.9, 0)	0.001	0.001	−0.016	−0.017	0.007	0.010	0.018	0.022	0.028	0.031	0.024	0.027
	t (3.9, 3.9, 3.9)	−0.004	−0.003	−0.010	−0.002	0.018	0.038	0.063	0.079	0.095	0.101	0.098	0.099
	T (9.6, 3.9, 3.9)	−0.004	−0.006	−0.021	−0.020	−0.016	−0.010	−0.003	−0.002	0.005	0.010	0.001	−0.002
Y	n (0, 0, 0)	−0.007	−0.011	−0.011	0.000	0.048	0.074	0.099	0.109	0.128	0.135	0.135	0.136
	u (3.9, 0, 0)	−0.001	−0.006	−0.005	0.009	0.061	0.092	0.124	0.150	0.175	0.179	0.186	0.185
	U (9.6, 0, 0)	−0.006	−0.007	0.000	0.013	0.074	0.105	0.140	0.160	0.181	0.189	0.195	0.200
	b (3.9, 3.9, 0)	−0.002	−0.001	−0.007	−0.007	0.009	0.018	0.028	0.031	0.036	0.038	0.034	0.035
	B (9.6, 3.9, 0)	0.000	0.000	−0.007	−0.007	0.015	0.019	0.029	0.032	0.037	0.042	0.037	0.037
	t (3.9, 3.9, 3.9)	−0.004	−0.002	−0.013	−0.006	0.001	0.011	0.027	0.029	0.040	0.043	0.038	0.038
	T (9.6, 3.9, 3.9)	−0.004	−0.005	−0.006	−0.001	0.009	0.017	0.027	0.029	0.039	0.046	0.042	0.039
Z	n (0, 0, 0)	−0.002	−0.005	−0.005	0.004	0.056	0.086	0.116	0.129	0.152	0.159	0.159	0.161
	u (3.9, 0, 0)	−0.006	−0.008	−0.007	0.007	0.061	0.094	0.131	0.160	0.188	0.193	0.201	0.200
	U (9.6, 0, 0)	−0.008	−0.008	0.003	0.018	0.080	0.114	0.152	0.176	0.200	0.209	0.216	0.220
	b (3.9, 3.9, 0)	−0.002	0.000	0.003	0.014	0.086	0.136	0.181	0.215	0.239	0.253	0.252	0.253
	B (9.6, 3.9, 0)	0.001	0.002	0.010	0.018	0.133	0.183	0.234	0.276	0.311	0.332	0.331	0.331
	t (3.9, 3.9, 3.9)	−0.003	−0.003	−0.015	−0.010	−0.005	0.001	0.014	0.022	0.032	0.035	0.033	0.032
	T (9.6, 3.9, 3.9)	−0.005	−0.006	−0.008	−0.007	0.001	0.010	0.020	0.028	0.038	0.045	0.039	0.037

the expansion measurement of the non-reactive specimens was subtracted from the corresponding measurement of the reactive specimen to obtain the net ASR expansion as presented in Table 3. (Note: the measurements for non-reactive specimens are not presented for brevity; they can be obtained by subtracting the values in Table 3 from values in Table 2). As can be seen in Table 2, the stress application, during 52 to 56 days of age, caused some elastic shortening in the cube specimens in the direction of the applied stress. Also, the ASR expansion until the age of stress application was insignificant as shown in Table 2. To exclude the effect of elastic shortening on the measure of ASR expansion, the net ASR expansion can thus be considered with reference to the post-loading measurement at 57 days as shown in Table 4. A scenario of triaxial expansions for all the stress states at the age of 545 days is presented in Fig. 2.

The results in Fig. 2 show that ASR axial expansion is reduced due to compressive stress and is transferred to free directions. For the specimens with uniaxial stress, the expansion was reduced in the x-direction, and the y- and z-directions had approximately identical expansions, which were however, greater than the corresponding y- and z-direction expansions of the no-stress specimens. For biaxially stressed specimens, the expansions were reduced in both of the stressed directions (x and y), and significantly greater expansion was observed in the unstressed (z) direction. Moreover, comparison of the z-direction (free direction) expansions of the biaxially stressed specimens b (3.9, 3.9, 0) and B (9.6,

3.9, 0) shows that the z-direction expansion increased with an increase in the stress level in the x-direction. For the triaxially stressed specimens, the axial expansions were markedly reduced in all three directions, resulting in lower volumetric expansion compared to the no-stress, uniaxial, and biaxial stress conditions. Compared to the other directions having identical stress, relatively larger expansion was observed in the x-direction of the b (3.9, 3.9, 0) and t (3.9, 3.9, 3.9) specimens, which is discussed in a subsequent section in relation to a non-uniform stress distribution.

Evolution of ASR expansion

The net ASR axial expansion results presented in Table 4 were used to calculate volumetric ASR expansion of the reactive specimens. The ratio of the volumetric expansion of concrete for each stress state to the volumetric expansion of concrete for no-stress state is presented in Fig. 3. The ratio for the triaxially stressed specimens was relatively smaller for the first month of accelerated curing (until an age of 210 days) than for the successive ages. However, the ratio of volumetric expansion remained fairly constant with age for all stress states. The volumetric expansion for uniaxially stressed specimens was mostly 90 to 118% of the volumetric expansion of the no-stress specimens. For biaxially stressed specimens, the volumetric expansion ranged from 90 to 99% of the volumetric expansion of no-stress specimens. However, the volumetric expansion was markedly reduced for the triaxially stressed specimens by approximately 50 to

Table 3—Net ASR axial expansion obtained after subtracting measurement of non-reactive specimens from reactive specimens, %

Axis	Age (days) → Stress state ↓	28	52	57	120	210	235	270	315	360	430	485	545
X	n (0, 0, 0)	−0.022	−0.016	−0.016	−0.012	0.030	0.069	0.099	0.102	0.114	0.122	0.125	0.124
	u (3.9, 0, 0)	−0.002	−0.007	−0.007	0.004	0.036	0.050	0.071	0.085	0.104	0.104	0.105	0.108
	U (9.6, 0, 0)	−0.024	−0.034	−0.031	−0.025	−0.014	−0.003	0.008	0.008	0.013	0.012	0.017	0.019
	b (3.9, 3.9, 0)	−0.015	−0.009	−0.010	−0.004	0.023	0.052	0.069	0.080	0.086	0.091	0.093	0.092
	B (9.6, 3.9, 0)	−0.010	−0.012	−0.015	−0.010	0.008	0.025	0.038	0.042	0.047	0.050	0.044	0.047
	t (3.9, 3.9, 3.9)	−0.012	−0.008	−0.008	−0.001	0.008	0.038	0.064	0.081	0.090	0.105	0.102	0.101
	T (9.6, 3.9, 3.9)	−0.020	−0.023	−0.024	−0.018	−0.024	−0.004	0.006	0.012	0.014	0.021	0.014	0.011
Y	n (0, 0, 0)	−0.025	−0.024	−0.024	−0.013	0.022	0.060	0.085	0.097	0.108	0.116	0.119	0.120
	u (3.9, 0, 0)	−0.008	−0.008	−0.008	0.006	0.058	0.089	0.122	0.146	0.173	0.178	0.181	0.182
	U (9.6, 0, 0)	−0.019	−0.024	−0.021	−0.010	0.051	0.080	0.115	0.133	0.153	0.158	0.164	0.168
	b (3.9, 3.9, 0)	−0.020	−0.013	−0.016	−0.011	−0.004	0.021	0.034	0.037	0.040	0.040	0.038	0.040
	B (9.6, 3.9, 0)	−0.010	−0.015	−0.016	−0.011	−0.002	0.013	0.027	0.029	0.032	0.038	0.034	0.034
	t (3.9, 3.9, 3.9)	−0.014	−0.001	−0.009	−0.003	−0.007	0.012	0.029	0.033	0.038	0.048	0.043	0.044
	T (9.6, 3.9, 3.9)	−0.020	−0.025	−0.026	−0.020	−0.022	−0.003	0.011	0.016	0.018	0.030	0.025	0.022
Z	n (0, 0, 0)	−0.015	−0.014	−0.014	−0.005	0.034	0.075	0.106	0.123	0.136	0.144	0.148	0.149
	u (3.9, 0, 0)	−0.008	−0.008	−0.008	0.005	0.061	0.092	0.131	0.159	0.187	0.193	0.196	0.197
	U (9.6, 0, 0)	−0.023	−0.028	−0.024	−0.007	0.054	0.083	0.119	0.143	0.165	0.171	0.179	0.183
	b (3.9, 3.9, 0)	−0.009	−0.005	−0.009	0.004	0.063	0.126	0.172	0.205	0.227	0.241	0.240	0.242
	B (9.6, 3.9, 0)	−0.009	−0.013	−0.011	−0.006	0.094	0.154	0.209	0.252	0.283	0.302	0.303	0.303
	t (3.9, 3.9, 3.9)	−0.012	−0.007	−0.005	0.001	−0.005	0.011	0.025	0.037	0.041	0.050	0.048	0.047
	T (9.6, 3.9, 3.9)	−0.019	−0.022	−0.025	−0.017	−0.022	0.000	0.012	0.023	0.028	0.037	0.031	0.029
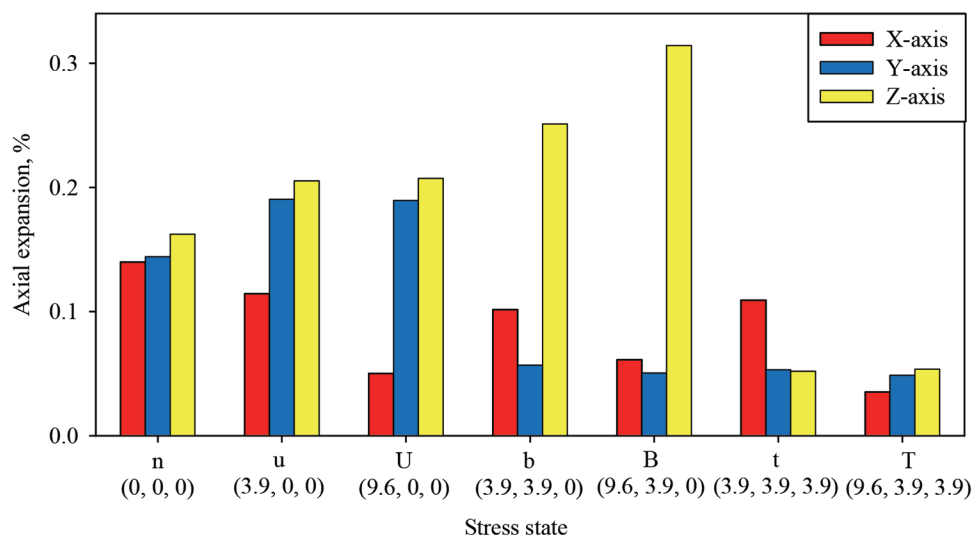
Fig. 2—Net ASR expansion in three directions for seven stress states at 545 days.

70%. Based on these observations, this study assumes that volumetric expansion due to ASR is conserved as long as there is at least one unstressed direction. This assumption is consistent with the understanding that ASR expansion is caused by the fluid pressure of the reaction products.[5,12,15,20-22]

Concrete samples were cut from the cube specimens and were examined microscopically after 56, 270, 430, and 545 days of casting. Figure 4 shows a digital microscope image of a polished surface of concrete from the t (3.9, 3.9, 3.9) specimen after 270 days of casting (90 days of accelerated curing). As exemplified in Fig. 4, reactive concrete specimens from all stress states experienced extensive ASR cracking after 90 days of accelerated curing. This illustrates that even though expansion was reduced, the reaction was not suppressed by the triaxial stress. Ichikawa and Miura[20] showed that the expansive pressure generated by ASR is

Table 4—Net ASR axial expansion with reference taken as measurement immediately after stress application, %

Axis	Age (days) → Stress state ↓	57	120	210	235	270	315	360	430	485	545
X	n (0, 0, 0)	0.000	0.004	0.046	0.085	0.115	0.118	0.130	0.139	0.141	0.140
	u (3.9, 0, 0)	0.000	0.011	0.043	0.057	0.078	0.092	0.111	0.111	0.112	0.114
	U (9.6, 0, 0)	0.000	0.006	0.017	0.028	0.039	0.039	0.043	0.043	0.048	0.050
	b (3.9, 3.9, 0)	0.000	0.006	0.032	0.062	0.079	0.090	0.096	0.101	0.103	0.102
	B (9.6, 3.9, 0)	0.000	0.005	0.023	0.039	0.053	0.057	0.061	0.065	0.059	0.061
	t (3.9, 3.9, 3.9)	0.000	0.007	0.016	0.045	0.071	0.089	0.098	0.113	0.110	0.109
	T (9.6, 3.9, 3.9)	0.000	0.006	0.001	0.020	0.031	0.036	0.038	0.045	0.038	0.035
Y	n (0, 0, 0)	0.000	0.011	0.047	0.084	0.109	0.122	0.132	0.140	0.144	0.144
	u (3.9, 0, 0)	0.000	0.014	0.067	0.098	0.130	0.155	0.182	0.186	0.190	0.190
	U (9.6, 0, 0)	0.000	0.011	0.072	0.101	0.136	0.154	0.174	0.179	0.185	0.189
	b (3.9, 3.9, 0)	0.000	0.005	0.013	0.037	0.051	0.053	0.056	0.057	0.055	0.057
	B (9.6, 3.9, 0)	0.000	0.005	0.014	0.029	0.043	0.045	0.048	0.054	0.050	0.050
	t (3.9, 3.9, 3.9)	0.000	0.006	0.003	0.021	0.039	0.042	0.048	0.058	0.052	0.053
	T (9.6, 3.9, 3.9)	0.000	0.007	0.004	0.024	0.038	0.042	0.044	0.056	0.052	0.049
Z	n (0, 0, 0)	0.000	0.008	0.048	0.089	0.119	0.136	0.150	0.158	0.162	0.162
	u (3.9, 0, 0)	0.000	0.013	0.069	0.100	0.139	0.166	0.195	0.201	0.204	0.205
	U (9.6, 0, 0)	0.000	0.017	0.078	0.107	0.143	0.167	0.189	0.195	0.203	0.207
	b (3.9, 3.9, 0)	0.000	0.013	0.072	0.135	0.181	0.214	0.236	0.250	0.249	0.251
	B (9.6, 3.9, 0)	0.000	0.005	0.105	0.165	0.221	0.263	0.294	0.314	0.314	0.314
	t (3.9, 3.9, 3.9)	0.000	0.006	0.000	0.015	0.030	0.042	0.045	0.055	0.053	0.052
	T (9.6, 3.9, 3.9)	0.000	0.008	0.003	0.025	0.037	0.048	0.053	0.062	0.056	0.054
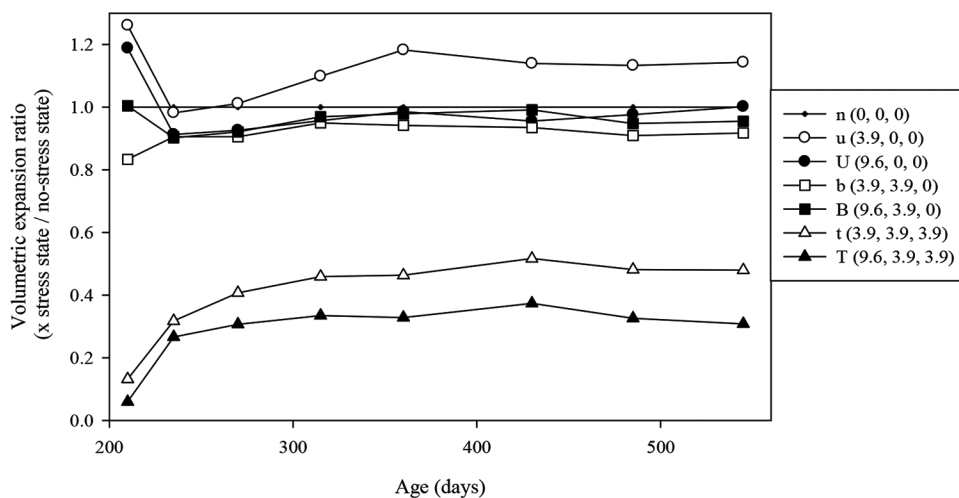
Fig. 3—Ratio of volumetric expansion for different stress states to volumetric expansion for no-stress state at different ages. (Note: "x" represents stress state n, u, U, b, B, t, or T.)

approximately 400 MPa (58 ksi). Thus, the stress state in concrete structures (approximately two orders of magnitude smaller) is unlikely to suppress the chemical reaction but can reduce ASR expansion. This mechanism can be convincingly explained by the theory of pressure-dependent filling of ASR gel in concrete pores.[5] Therefore, an increase in stress causes ASR gel to penetrate into the increasingly smaller micro-pores in concrete. Even though Takahashi et al.[5] proposed the theory even for the case of uniaxial stress, the experimental results in this study showed that the theory is applicable for the case of triaxial confinement. In the case of uniaxial or biaxial confinement, as the reaction product can preferentially flow towards the unstressed direction, the pressure gradient is perhaps inadequate to make it penetrate into the micro-pores.

Figure 5 shows the evolution of volumetric expansion with age for the seven stress states. The volumetric expansion is plotted as a ratio of its value at an age to that at 545 days. The evolution of volumetric expansion with age appears to be identical irrespective of the stress state with the exception of two observations. First, the evolution of volumetric expansion in the triaxially stressed specimens was delayed by approximately 1 month. The pressure-dependent filling of ASR gel in concrete in the triaxially stressed specimens might have contributed to this delay. Also, relatively less exposure of concrete to moisture due to the presence of plates in all directions could have influenced to some extent. However, these mechanisms were not experimentally verified in this study. Second, the triaxially stressed specimens—particularly T (9.6, 3.9, 3.9)—experienced some contraction after the peak expansion at 430 days. Despite these exceptions, overall, the evolution in volumetric expansion in Fig. 5 indicates a characteristic sigmoidal curve for ASR expansion as proposed by Larive[4] and Ulm et al.[12] This observation suggests that the effect of stress state on reaction kinetics can be practically ignored. Thus, this paper postulates that reaction kinetics can be decoupled from the effect of stress state.

Stress distribution and its effect on expansion

Table 5 presents the net ASR axial expansion of cubes along x-, y-, and z-directions as the percentage of volumetric expansion of the no-stress specimens at corresponding ages. The data are shown for the age range of 315 to 545 days, in which the ratio of volumetric expansion for a stress state to that for no-stress state remained relatively constant as shown in Fig. 3.

As shown in Table 5, for an average stress of 3.9 MPa (566 psi) in the y-direction, the y-direction expansions of the biaxially stressed (b and B) specimens are approximately

similar from 315 to 545 days. Similarly, for an average stress of 3.9 MPa (566 psi) in the y- and z-directions, the y- and z-direction expansions of the triaxially stressed (t and T) specimens are approximately identical. For an average stress of 3.9 MPa (566 psi) in the x-direction, the x-direction expansions of the stressed (u, b, and t) specimens are approximately identical; however, they are approximately double the y-direction expansions of the biaxially stressed (b and B) specimens, with an average stress of 3.9 MPa (566 psi) in the y-direction, and of the y- and z-direction expansions of the triaxially stressed (t and T) specimens, with an average stress of 3.9 MPa (566 psi) each in the y- and z-directions. For an average stress of 9.6 MPa (1392 psi) in the x-direction,
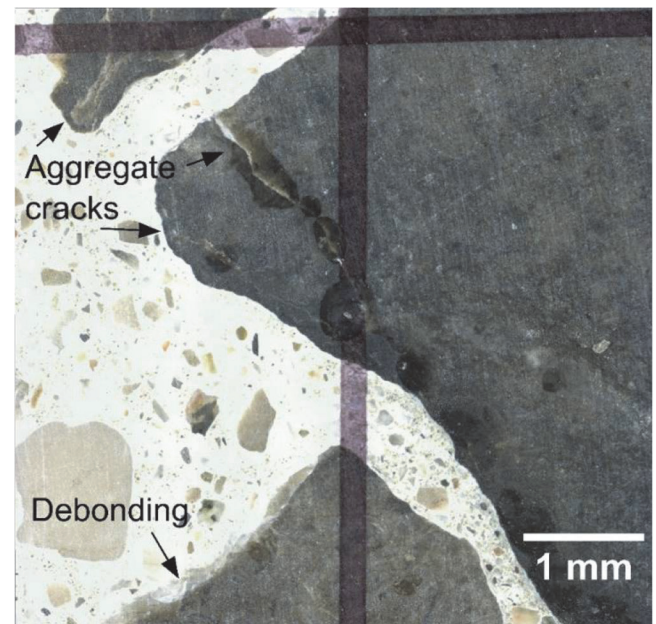

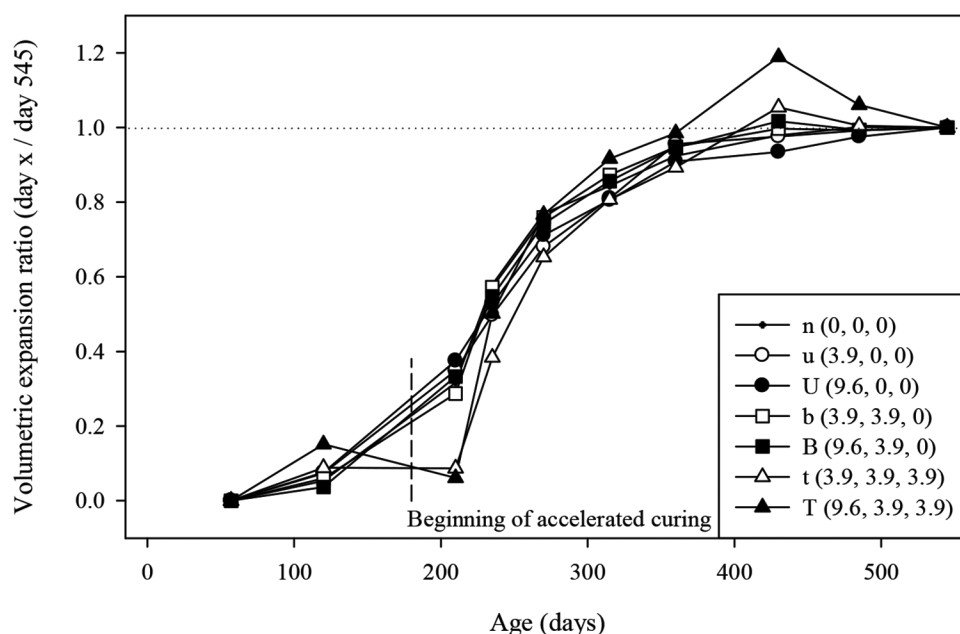Fig. 4—ASR cracks on polished surface of concrete from t (3.9, 3.9, 3.9) specimen. (Note: 1 mm = 0.039 in.)

Fig. 5—Evolution of volumetric expansion with age for seven stress states. (Note: volumetric expansion is plotted as ratio of its value at age "x" days to that at 545 days.)

Table 5—Net ASR axial expansion as percentage of volumetric expansion of no-stress specimens

Axis	Age (days) → Stress state ↓	315	360	430	485	545
X	n (0, 0, 0)	31.4	31.6	31.7	31.6	31.3
	u (3.9, 0, 0)	24.5	26.9	25.3	25.1	25.6
	U (9.6, 0, 0)	10.3	10.5	9.9	10.7	11.3
	b (3.9, 3.9, 0)	24.0	23.2	23.2	22.9	22.8
	B (9.6, 3.9, 0)	15.1	14.9	14.9	13.2	13.7
	t (3.9, 3.9, 3.9)	23.6	23.8	25.9	24.6	24.5
	T (9.6, 3.9, 3.9)	9.6	9.3	10.4	8.6	7.9
Y	n (0, 0, 0)	32.3	32.1	32.1	32.2	32.3
	u (3.9, 0, 0)	41.1	44.1	42.7	42.4	42.7
	U (9.6, 0, 0)	41.0	42.1	41.0	41.4	42.5
	b (3.9, 3.9, 0)	14.2	13.7	13.0	12.3	12.7
	B (9.6, 3.9, 0)	11.9	11.7	12.4	11.2	11.3
	t (3.9, 3.9, 3.9)	11.3	11.5	13.2	11.7	11.9
	T (9.6, 3.9, 3.9)	11.2	10.8	12.8	11.6	10.9
Z	n (0, 0, 0)	36.2	36.3	36.2	36.2	36.4
	u (3.9, 0, 0)	44.2	47.3	45.9	45.7	46.0
	U (9.6, 0, 0)	44.4	45.9	44.7	45.5	46.5
	b (3.9, 3.9, 0)	56.8	57.3	57.2	55.7	56.3
	B (9.6, 3.9, 0)	69.9	71.3	71.8	70.3	70.4
	t (3.9, 3.9, 3.9)	11.0	11.0	12.6	11.8	11.6
	T (9.6, 3.9, 3.9)	12.7	12.7	14.2	12.5	12.0

the x-direction expansions of the stressed (U, B, and T) specimens are comparable.

The relatively larger expansion in the x-direction of the u (3.9, 0, 0), b (3.9, 3.9, 0) and t (3.9, 3.9, 3.9) specimens is attributed to the non-uniform stress distribution along the x-direction. Since the expansion measurement studs in the x-direction were relatively farther from the smaller bearing plates as shown in Fig. 1(a), the measured expansion at the studs was contributed by both the uniformly stressed core concrete and the low-stressed near-surface concrete. The stress distribution along the axes of expansion measurement studs of the u (3.9, 0, 0), b (3.9, 3.9, 0) and t (3.9, 3.9, 3.9) specimens were obtained by a finite element analysis performed using VecTor3 program. VecTor3 is a non-linear finite element analysis software developed at the University of Toronto for the analysis of 3-D reinforced concrete structures.[23]

Based on the VecTor3 analysis, Fig. 6 shows the distribution of normal stress in the x-direction (f_x) on the two planes XY and XZ of the t (3.9, 3.9, 3.9) specimen passing through the axis of the expansion measurement stud "X1" (X1 is one of the four expansion measurement studs in the x-direction, as shown in Fig. 1(b)). The stress concentration caused by the bearing plates is evident.

Stress distribution along the two stud axes X1 and X2, as shown in Fig. 1(b) (because of symmetry, X3 and X4 would be identical to X1 and X2, respectively), was obtained from

the VecTor3 analysis. To obtain the average nodal stress along the stud axis, nodal stress values for the stud axes X1 and X2 were averaged between the nodes having identical x-coordinates. Figure 7 shows a plot of the nodal stress distributions in the x-direction along the stud axis (gauge length) for the u (3.9, 0, 0), b (3.9, 3.9, 0), and t (3.9, 3.9, 3.9) specimens. Then, average stress along the stud axis was taken as the nodal stress averaged over the gauge length. The average stress in the x-direction along the stud axis was 2.6 ± 0.1 MPa (377 ± 8 psi), 2.2 ± 0.6 MPa (319 ± 80 psi) and 1.7 ± 0.3 MPa (247 ± 49 psi), respectively, for the u (3.9, 0, 0), b (3.9, 3.9, 0), and t (3.9, 3.9, 3.9) specimens. Lower stress was observed from u (3.9, 0, 0) to b (3.9, 3.9, 0) to t (3.9, 3.9, 3.9) specimens. This was due to Poisson effect caused by the stress in the y-direction in the b (3.9, 3.9, 0) specimen and the stresses in the y- and z-directions in the t (3.9, 3.9, 3.9) specimen. In addition to the stress in the x-direction, stresses along the stud axes in the y- and z-directions of the b (3.9, 3.9, 0) and t (3.9, 3.9, 3.9) specimens were also analyzed. The average stress in the y-direction along the stud axis of the b (3.9, 3.9, 0) and t (3.9, 3.9, 3.9) specimens, taken together, was 2.9 ± 0.8 MPa (420 ± 123 psi) and the average stress in the z-direction along the stud axis of the t (3.9, 3.9, 3.9) specimen was approximately 3.1 ± 0.4 MPa (450 ± 60 psi).

MULTIAXIAL EXPANSION-STRESS RELATIONSHIP

Based on the experimental results and the stress analysis of the specimens, a relationship between expansion and stress is proposed in this study. Because ASR expansion can transfer from one direction to another depending on the stress state, ASR expansion in a direction is governed not only by the stress in the given direction but also by the stresses in the other two directions. Thus, a given direction can have a range of ASR expansion corresponding to a free volumetric expansion. The range is defined as [pe_{un}, pe_{max}], where pe_{un} represents the "uncoupled axial expansion" in the direction and pe_{max} represents the "maximum possible axial expansion" in the direction. (It should be noted that the term "uncoupled" here means the axial expansion is not coupled with the stresses in the other directions). These two expansions are further described in subsequent sections.

Fairly identical expansions in the x-direction for the u (3.9, 0, 0), b (3.9, 3.9, 0) and t (3.9, 3.9, 3.9) specimens indicate that no additional expansion due to transfer is possible (no coupling of expansion in the x-direction with stresses in the y- and z-directions) for the level of stress in the x-direction in these specimens. Thus, additional expansion in a given direction due to transfer of expansion from other directions is assumed to be possible only for no stress or a relatively lower stress (<1.7 MPa [247 psi]) in the direction.

Uncoupled axial expansion

A slightly greater z-direction expansion than the x- and y-direction expansions in the no-stress specimen was attributed to the anisotropy associated with casting direction[24] and was ignored for modeling purposes. Therefore, the uncoupled axial expansion for no-stress specimen was considered as one-third (33.3%) of the volumetric expan-

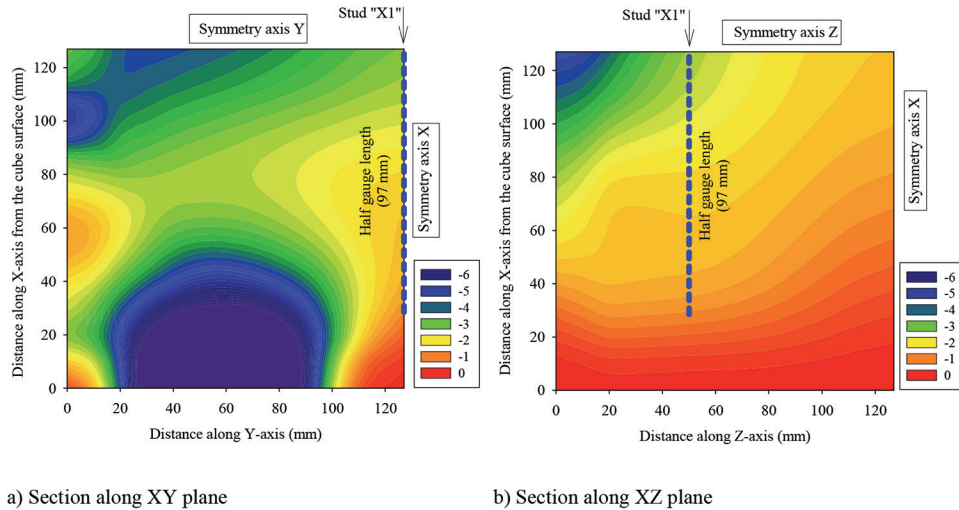a) Section along XY plane   b) Section along XZ plane

Fig. 6—Distribution of normal stress f_x *(MPa) in one-eighth of t (3.9, 3.9, 3.9) specimen in XY and XZ planes containing expansion measurement stud "X1" in x-direction. (Note: 1 mm = 0.039 in.; 1 MPa = 145 psi.)*

sion of no-stress specimen. The volumetric expansion of the no-stress specimen is hereafter referred to as free volumetric expansion. The expansion in the x-direction of the u (3.9, 0, 0), b (3.9, 3.9, 0), and t (3.9, 3.9, 3.9) specimens was identical as shown in Table 5, and the average value was 24.5% of the free volumetric expansion. This expansion was attributed to the 1.7 MPa (247 psi) stress (among the three stress levels of 1.7, 2.2, and 2.6 MPa [247, 319, and 377 psi], 1.7 MPa [247 psi] was found most appropriate as verified during trial analysis). The expansion in the y-direction of the b (3.9, 3.9, 0), B (9.6, 3.9, 0), t (3.9, 3.9, 3.9), and T (9.6, 3.9, 3.9) specimens and the expansion in the z-direction of the t (3.9, 3.9, 3.9) and T (9.6, 3.9, 3.9) specimens, all with an average stress of 3.0 MPa (435 psi), was comparable, and the average uncoupled axial expansion, as obtained from Table 5, was 12.1% of the free volumetric expansion. The expansion in the x-direction of the U (9.6, 0, 0), B (9.6, 3.9, 0), and T (9.6, 3.9, 3.9) specimens, which have an average stress of 9.6 MPa (1392 psi) in the x-direction, was comparable, and the average uncoupled axial expansion, as obtained from Table 5, was 11.4% of the free volumetric expansion. Hence, the experiment provided four points for the expansion-stress curve, namely, four stresses—0, 1.7, 3.0 and 9.6 MPa—with corresponding uncoupled axial expansions of 33.3, 24.5, 12.1 and 11.4%, respectively, of the free volumetric expansion. The change in expansion corresponding to the stresses of 3.0 and 9.6 MPa (435 and 1392 psi) was extremely small. On the other hand, the difference in expansion corresponding to the stresses of 1.7 and 3.0 MPa (247 and 435 psi) was quite large. These observations indicate that the expansion-stress curve has a reverse S-shaped pattern, in which ASR expansion is extremely sensitive to stress in a range around 1.7 MPa (247 psi) and is less sensitive for stresses greater than that. A relatively smaller stress, in the range of 0.3 MPa (43.5 psi), has been considered as insignificant to reduce any ASR expansion.[3,14] Moreover, a uniaxial test by Kagimoto et al.[2] indicated that the expansive pressure generated by ASR gel is stabilized at a stress level of approximately 2.6 MPa
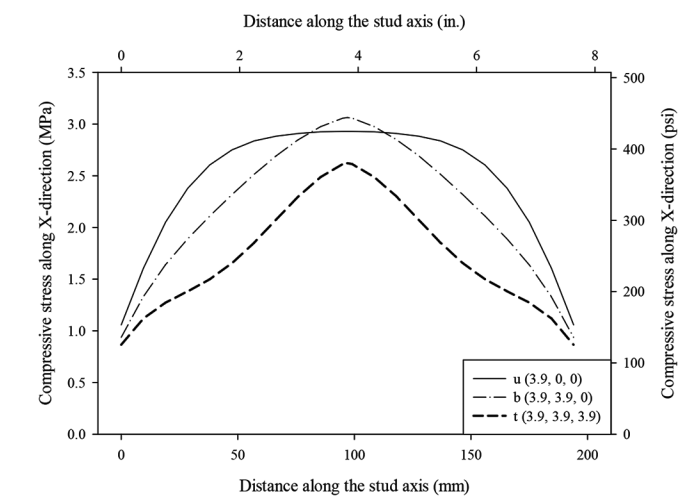

Fig. 7—Stress distribution along stud axis in x-direction for u (3.9, 0, 0), b (3.9, 3.9, 0), and t (3.9, 3.9, 3.9) specimens.

(377 psi). Based on the experimental results and considering the literature observations,[2,3] curve fitting was performed to obtain a relationship between the stress and expansion in a given direction. The model that best suited the data in this study was a four-parameter logistic curve as below

$$pe_{un} = a + \frac{b-a}{1+\left(\dfrac{f}{c}\right)^d} \quad \text{for } f \geq 0 \qquad (1)$$

where pe_{un} is the uncoupled axial expansion in a given direction expressed as the percentage of free volumetric expansion; a, b, c, and d are constants of curve-fitting; and f is the stress in MPa (note: 1 MPa = 145 psi) in the given direction where compression is positive. The constants a, b, c, and d were obtained to be 11.4, 33.3, 1.8, and 6.5, respectively. Equation (1) indicates that an axial expansion of 11.4% of the free volumetric expansion will occur despite a large compressive stress. This observation should, however, be interpreted considering the experimental setup considered in this study.
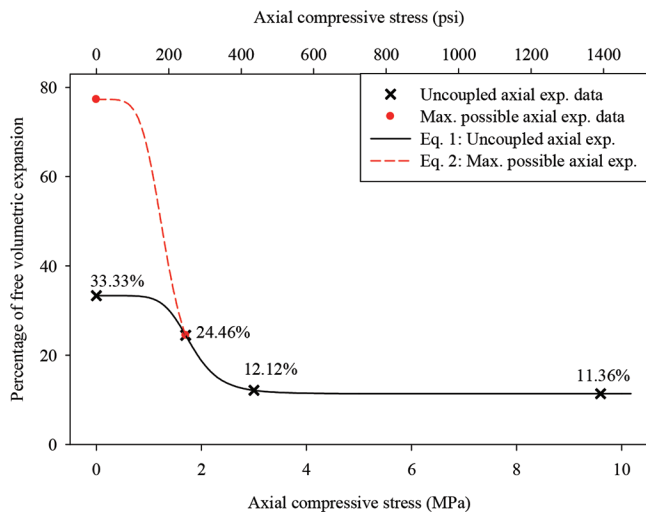
Fig. 8—Relationship of ASR expansion with stress.

Maximum possible axial expansion

For the range of stress from 0 to 1.7 MPa (0 to 247 psi), ASR expansion in a given direction is influenced by the stresses in the other directions. Thus, the expansion can have a range from an uncoupled axial expansion to the maximum possible axial expansion. Because volumetric expansion is assumed to conserve for a biaxial stress state, the axial expansion in the unstressed direction in a restrained specimen can be substantially larger than in a no-stress specimen. Based on Eq. (1) for a biaxial stress state, considering the two stressed directions will have an expansion of at least 11.4% of the free volumetric expansion, the maximum possible axial expansion in the free direction can be 77.2% (= 100 – 2 × 11.4%) of the free volumetric expansion. This value was considered as the maximum possible axial expansion in the free direction. The maximum possible axial expansion was considered the same as the uncoupled axial expansion for stresses exceeding 1.7 MPa (247 psi). No experimental expansion data were available corresponding to stress levels between 0 and 1.7 MPa (0 and 247 psi). Therefore, a logistic function was assumed for the maximum possible axial expansion as for the uncoupled axial expansion. Thus, a four-point logistic curve was fitted for four points; namely, four stresses—0, 1.7, 3.0, and 9.6 MPa—with corresponding maximum possible axial expansions as 77.2, 24.5, 12.1, and 11.4%, respectively, of the free volumetric expansion. The equation for the maximum possible axial expansion pe_{max}, expressed as the percentage of free volumetric expansion, is given as

$$pe_{max} = A + \frac{B - A}{1 + \left(\dfrac{f}{C}\right)^{D}} \text{ for } f \geq 0 \qquad (2)$$

where constants A, B, C, and D are 11.4, 77.2, 1.3, and 5.4, respectively.

The uncoupled and the maximum possible axial expansions, as obtained from Eq. (1) and (2), respectively, are plotted in Fig. 8. Because the two curves overlap for stress exceeding 1.7 MPa (247 psi), Eq. (2) need only be used for stress range from 0 to 1.7 MPa (0 to 247 psi).

The stress states involved in the experimental study were only compressive. Thus, the scenario of ASR expansion for tensile stress needs further research. For this study, ASR expansion in a direction with tensile stress was considered same as for unstressed direction.

Expansion distribution along three directions

If the sum of maximum possible axial expansion in three directions is less than 100% (that is, equal to the free volumetric expansion), the expansion in each direction will be equal to the maximum possible axial expansion in the respective direction. If the sum of maximum possible axial expansion in the three directions is greater than the free volumetric expansion, the volumetric expansion will not be reduced and will be limited to the free volumetric expansion. The difference between 100% and the sum of the uncoupled axial expansion in three directions needs to be distributed along the three directions. The relative weights of the distribution will depend on the stress state in each direction. The ASR expansion that needs to be distributed is proposed to be distributed proportional to the difference in the maximum possible axial expansion and the uncoupled axial expansion ($pe_{max} - pe_{un}$) for each direction.

VALIDATION

The proposed expansion-stress relationship was implemented in the finite element analysis program, VecTor3, by Jurcut.[23] ASR expansion in VecTor3 program is modeled as fixed orthotropic elastic strain offsets.[23] The ASR-induced strain, which can depend on the stress state of concrete, is evaluated following an iterative procedure.[23] The specimens u (3.9, 0, 0), b (3.9, 3.9, 0), and t (3.9, 3.9, 3.9) from the experiment were analyzed in VecTor3 program to validate the proposed expansion-stress relationship. Before performing an actual analysis, trial analyses were performed on simple one-element and multi-element models to confirm that the expansion-stress relationship implemented in the program behaved reasonably.

Figure 9 shows a typical model of the t (3.9, 3.9, 3.9) specimen in VecTor3. The dark blue color represents the steel plate, the light blue color represents concrete, the white shade represents a dummy material with extremely low strength and stiffness, and the red arrows represent the loading (please refer to the online version for the color representation of the figure). Because of symmetry, only one-eighth of the cube specimen was modeled. Brick elements were used to model concrete and steel plate. Concrete was modeled with 14 elements along a direction. Based on the results from tests of concrete cylinders and cores, the compressive strength, modulus of elasticity, and Poisson's ratio of concrete were given as 44.2 MPa (6.4 ksi), 29 GPa (4205 ksi), and 0.2, respectively. Steel plates were modeled with two elements through the thickness and the load was applied on top of the bearing plates distributed at eight nodes, approximately representing the washer used in the experiment. Due to a simplification in modeling, a bearing plate had a slight discrepancy in its position (maximum 4 mm [0.16 in.]) and orientation relative to the experimental configuration. The experiment involved 12 friction-less steel sheaths in the 12
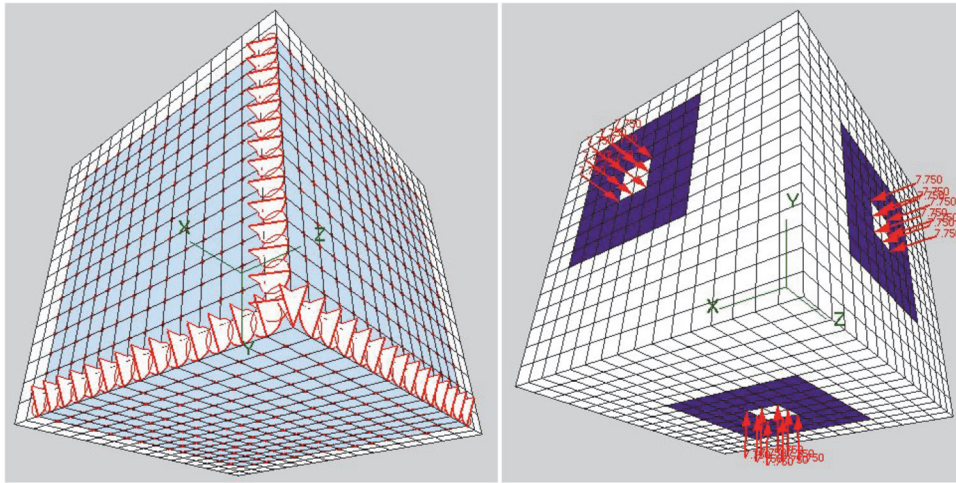
Fig. 9—VecTor3 model of triaxial t (3.9, 3.9, 3.9) specimen.

holes in concrete designed for passing the bolts. The sheaths and the holes were not modeled in the VecTor3 model.

Figure 10 compares the numerical results with the experimental results for the u (3.9, 0, 0), b (3.9, 3.9, 0), and t (3.9, 3.9, 3.9) specimens. Because the experimental results are net ASR expansion, the numerical results for ASR expansion also consider net ASR expansion. For this, two sets of numerical analysis were performed for each case: one with ASR expansion and the other without ASR expansion. Figure 10 shows that the results from the numerical analysis are in good agreement with the experimental results. Moreover, Fig. 10 also compares the numerical results obtained using the Saouma and Perotti[17] model for an identical free volumetric expansion. The results from the model presented in this study are markedly closer to the experimental results for the uniaxial, biaxial and triaxial stress states compared to those from the Saouma and Perotti[17] model.

Fig. 10—Expansion of cube specimens u (3.9, 0, 0), b (3.9, 3.9, 0), and t (3.9, 3.9, 3.9) from numerical analyses and experiment at 545 days.

DISCUSSION

The proposed empirical model was validated against the experimental measurements for cube specimens having multiaxial stress states. The arrangement for stress application in the experiment caused non-uniform stress distribution in the cube specimens. However, the stress distribution was obtained by a numerical analysis, and the stress condition helped in formulating and validating the expansion-stress relationship. A small discrepancy might have occurred due to the simplifications made in the numerical analysis; namely, no consideration of the sheaths and the holes in concrete, and a slight dislocation of bearing plate relative to the experimental case. The degradation of concrete properties due to ASR has not been incorporated in the proposed expansion-stress relationship. Appropriate degradation parameters corresponding to the free volumetric expansion and the stress state of concrete may be specified in an analysis program, as required.

The proposed model decouples ASR from creep simply based on experiments involving non-reactive concrete. More complicated experimental investigation to decouple the ASR and creep strains in reactive concrete can be a topic of future research interest. Additionally, the present model decou-
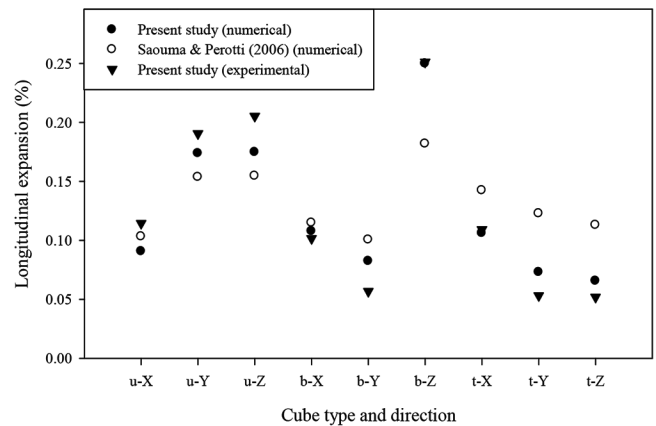
ples the effect of stress on the reaction kinetics based on the experimental observation. This consideration greatly simplifies the simulation of ASR-affected concrete structures. The present model can be used for a given free volumetric expansion and should be adequate for most structural applications. However, if the evolution of structural performance is to be examined, the present model may still be used by giving the free volumetric expansion in several increments and by considering the stress state at each increment.

The proposed model indicates that a minimum axial expansion of 11.4% of the free volumetric expansion will occur despite a large compressive stress. This appears unreasonable for a relatively larger compressive stress. However, for the typical stress level in concrete structures, which is mostly below 10 MPa (1.45 ksi), this level of expansion may not be unreasonable and is conservative. Furthermore, a stress level of approximately 1.5 MPa (217 psi) corresponds to an uncoupled axial expansion of 28.4% and the maximum possible axial expansion of 33.3% of the free volumetric expansion. Thus, based on the model, a hydrostatic stress state lower than 1.5 MPa (217 psi) cannot reduce volumetric ASR expansion.

The ASR expansion transfers from a stressed direction to a relatively less stressed direction. The expansion transfer

mechanism as observed in the experimental study revealed a tendency approximately analogous to the expansion of fluid. Thus, any attempts to interpret ASR expansion based on the concept of the first invariant of the stress tensor are not valid. For instance, the first invariant of the stress tensor for the B (9.6, 3.9, 0) specimen is greater than that for the t (3.9, 3.9, 3.9) specimen. However, the volumetric expansion of the B (9.6, 3.9, 0) specimen was practically not reduced but the volumetric expansion of the t (3.9, 3.9, 3.9) specimen was reduced by 50%. Additionally, even though the experiment showed the expansion transfer effect in the uniaxial and biaxial specimens, the number of cases in this study were still insufficient to clearly define transfer as a function of stress state. Further studies are needed to focus on additional stress levels, particularly in the range of 0.5 to 2 MPa (72 to 290 psi).

Finally, the proposed model is based on one reactive concrete mixture. Based on the strength and pore structure of concrete and the type of reactive aggregate, some variations may be possible for other concrete mixtures, particularly on the empirical constants. Also, in slender members, transfer of expansion may be influenced to some extent due to the aspect ratio of the structures.

CONCLUSION

A relationship between ASR expansion and stress state was proposed based on an experimental study that measured the ASR expansion in the three mutually perpendicular directions in a number of unrestrained and restrained concrete cube specimens subjected to uniaxial, biaxial, or triaxial stresses. The experimental results showed: (i) the reduction of ASR expansion due to stress; (ii) the transfer of ASR expansion from stressed to unstressed direction; and (iii) the reduction in volumetric expansion due to triaxial stress. Moreover, the reaction kinetics was not coupled with the expansion-stress relationship. Therefore, the proposed empirical relationship is not coupled with the reaction kinetics. The relationship is simple to implement in a numerical analysis program. It was implemented in a finite element analysis program, VecTor3. The relationship was validated with the experimental results in cube specimens with uniaxial, biaxial and triaxial stress states. Rooted in an experimental investigation involving the measurement of ASR expansion for the case of multiaxial stress states, this model is expected to be an accurate basis for reliably estimating the ASR expansion of concrete structures in multiple directions.

AUTHOR BIOS

ACI member **Bishnu Prasad Gautam** *received his PhD from the University of Toronto, Toronto, ON, Canada, in 2016; his ME from the University of Tokyo, Tokyo, Japan; and his BE from Tribhuvan University, Kirtipur, Nepal. He was the recipient of the Ontario Chapter – ACI 2012 Nick Bada Ontario Chapter Graduate Scholarship. His research interests include the materials and mechanics aspects of concrete structures and the application of precast and prestressed concrete.*

ACI member **Daman K. Panesar** *is an Associate Professor in the Department of Civil Engineering at the University of Toronto. Her research interests include advancing concrete materials, low carbon materials, material characterization and durability performance of aging infrastructure.*

Shamim A. Sheikh, *FACI, is a Professor of Civil Engineering at the University of Toronto. He is a member of ACI Committee 374, Performance-Based Seismic Design of Concrete Buildings, and former Chair and member of Joint ACI-ASCE Committee 441, Reinforced Concrete Columns. In 1999, he received the ACI Chester Paul Seiss Award for Excellence in Structural Research. His research interests include earthquake resistance and design of concrete structures, concrete confinement, and use of fiber-reinforced polymer for sustainable concrete structures.*

Frank J. Vecchio, *FACI, is a Professor in the Department of Civil Engineering at the University of Toronto. He is a member of Joint ACI-ASCE Committees 441, Reinforced Concrete Columns, and 447, Finite Element Analysis of Reinforced Concrete Structures. He was a recipient of the ACI Chester Paul Siess Award for Excellence in Structural Research in 1998, the ACI Design Award in 1999, the ACI Wason Medal for Most Meritorious Paper in 2011, and the ACI Joe W. Kelly Award in 2016. His research interests include advanced constitutive modeling and analysis of reinforced concrete, and assessment and rehabilitation of damaged or deficient structures.*

REFERENCES

1. Doran, D.; Douglas, J.; and Pratley, R., *Refurbishment and Repair in Construction*, Whittles Publishing, Dunbeath, UK, 2009, 314 pp.

2. Kagimoto, H.; Yasuda, Y.; and Kawamura, M., "ASR Expansion, Expansive Pressure and Cracking in Concrete Prisms under Various Degrees of Restraint," *Cement and Concrete Research*, V. 59, No. 5, 2014, pp. 1-15. doi: 10.1016/j.cemconres.2014.01.018

3. Berra, M.; Faggiani, G.; Mangialardi, T.; and Paolini, A. E., "Influence of Stress Restraint on the Expansive Behaviour of Concrete Affected by Alkali-Silica Rreaction," *Cement and Concrete Research*, V. 40, No. 9, 2010, pp. 1403-1409. doi: 10.1016/j.cemconres.2010.05.002

4. Larive, C., "Combined Contribution of Experiments and Modelling to the Understanding of Alkali-Aggregate Reaction and its Mechanical Consequences," PhD thesis, Ecole Nationale des Ponts et Chausses, Marne-la-Vallée, France, 1998. (in French)

5. Takahashi, Y.; Shibata, K.; Maruno, M.; and Maekawa, K., "Uniaxial Restraint Tests under High-Stress Conditions and a Chemo-Hygral Model for ASR Expansion," *Proceedings of the 10th International Conference on Mechanics and Physics of Creep, Shrinkage, and Durability of Concrete and Concrete Structures*, Vienna, Austria, Sept. 2015, pp. 1061-1065.

6. Dunant, C. F., and Scrivener, K. L., "Effects of Uniaxial Stress on Alkali-Silica Reaction Induced Expansion of Concrete," *Cement and Concrete Research*, V. 42, No. 3, 2012, pp. 567-576. doi: 10.1016/j.cemconres.2011.12.004

7. Gravel, C.; Ballivy, G.; Khayat, K.; Quirion, M.; and Lachemi, M., "Expansion of AAR Concrete under Triaxial Stresses—Simulation with Instrumented Concrete Block," *11th International Conference on Alkali Aggregate Reaction*, Quebec City, QC, Canada, June 2000, pp. 959-968.

8. Multon, S., and Toutlemonde, F., "Effect of Applied Stresses on Alkali-Silica Reaction-Induced Expansions," *Cement and Concrete Research*, V. 36, No. 5, 2006, pp. 912-920. doi: 10.1016/j.cemconres.2005.11.012

9. Gautam, B. P., and Panesar, D. K., "A New Method of Applying Long-Term Multiaxial Stresses in Concrete Specimens undergoing ASR, and their Triaxial Expansions," *Materials and Structures*, V. 49, No. 9, 2016, pp. 3495-3508. doi: 10.1617/s11527-015-0734-z

10. Dunant, C. F., and Scrivener, K. L., "Physically Based Models to Study the Alkali-Silica Reaction," *Proceedings of the Institution of Civil Engineers—Construction Materials*, V. 169, No. 3, 2016, pp. 136-144. doi:10.1680/jcoma.15.00073.10.1680/jcoma.15.00073

11. Saouma, V.; Perotti, L.; and Shimpo, T., "Stress Analysis of Concrete Structures Subjected to Alkali-Aggregate Reactions," *ACI Structural Journal*, V. 104, No. 5, Sept.-Oct. 2007, pp. 532-541.

12. Ulm, F.; Coussy, O.; Kefei, L.; and Larive, C., "Thermo-Chemo-Mechanics of ASR Expansion in Concrete Structures," *Journal of Engineering Mechanics*, ASCE, V. 126, No. 3, 2000, pp. 233-242. doi: 10.1061/(ASCE)0733-9399(2000)126:3(233)

13. Huang, M., and Pietruszczak, S., "Modeling of Thermomechanical Effects of Alkali-Silica Reaction," *Journal of Engineering Mechanics*, ASCE, V. 125, No. 4, 1999, pp. 476-485. doi: 10.1061/(ASCE)0733-9399(1999)125:4(476)

14. Léger, P.; Cote, P.; and Tinawi, R., "Finite Element Analysis of Concrete Swelling Due to Alkali-Aggregate Reactions in Dams," *Computers & Structures*, V. 60, No. 4, 1996, pp. 601-611. doi: 10.1016/0045-7949(95)00440-8

15. Grimal, E.; Sellier, A.; Pape, Y. L.; and Bourdarot, E., "Creep, Shrinkage, and Anisotropic Damage in Alkali-Aggregate Reaction Swelling Mechanism—Part I: A Constitutive Model," *ACI Materials Journal*, V. 105, No. 3, May-June 2008, pp. 227-235.

16. Capra, B., and Sellier, A., "Orthotropic Modelling of Alkali-Aggregate Reaction in Concrete Structures: Numerical Simulations," *Mechanics of Materials*, V. 35, No. 8, 2003, pp. 817-830. doi: 10.1016/S0167-6636(02)00209-0

17. Saouma, V., and Perotti, L., "Constitutive Model for Alkali-Aggregate Reactions," *ACI Materials Journal*, V. 103, No. 3, May-June 2006, pp. 194-202.

18. ASTM C1293-08, "Standard Test Method for Determination of Length Change of Concrete Due to Alkali-Silica Reaction," ASTM International, West Conshohocken, PA, 2008, 7 pp.

19. Gautam, B. P., "Multiaxially Loaded Concrete Undergoing Alkali-Silica Reaction (ASR)," PhD thesis, University of Toronto, Toronto, ON, Canada, 2016, 187 pp.

20. Ichikawa, T., and Miura, M., "Modified Model of Alkali-Silica Reaction," *Cement and Concrete Research*, V. 37, No. 9, 2007, pp. 1291-1297. doi: 10.1016/j.cemconres.2007.06.008

21. Sanchez, L. F. M.; Multon, S.; Sellier, A.; Cyr, M.; Fournier, B.; and Jolin, M., "Comparative Study of a Chemo-Mechanical Modeling for Alkali Silica Reaction (ASR) with Experimental Evidences," *Construction & Building Materials*, V. 72, 2014, pp. 301-315. doi: 10.1016/j.conbuildmat.2014.09.007

22. Rajabipour, F.; Giannini, E.; Dunant, C. F.; Ideker, J. H.; and Thomas, M. D. A., "Alkali-Silica Reaction: Current Understanding of the Reaction Mechanisms and the Knowledge Gaps," *Cement and Concrete Research*, V. 76, 2015, pp. 130-146. doi: 10.1016/j.cemconres.2015.05.024

23. Jurcut, A., "Modelling of the Effects of Alkali-Aggregate Reaction in Reinforced Concrete Structures," master's thesis, University of Toronto, Toronto, ON, Canada, 2015, 124 pp.

24. Smaoui, N.; Berube, M.; Fournier, B.; and Bissonnette, B., "Influence of Specimen Geometry, Orientation of Casting Plane, and Mode of Concrete Consolidation on Expansion Due to ASR," *Cement, Concrete and Aggregates*, V. 26, No. 2, 2004, pp. 58-70. doi: 10.1520/CCA11927

Table A1—Standard deviation of as-measured axial expansion of reactive specimens, %

Axis	Stress state ↓	28	52	57	120	210	235	270	315	360	430	485	545
X	n (0, 0, 0)	0.006	0.008	0.007	0.009	0.016	0.019	0.023	0.012	0.021	0.015	—	—
	u (3.9, 0, 0)	0.004	0.004	0.006	0.010	0.008	0.011	0.017	0.017	0.016	0.016	—	—
	U (9.6, 0, 0)	0.002	0.002	0.003	0.002	0.004	0.005	0.005	0.000	0.004	0.003	—	—
	b (3.9, 3.9, 0)	0.012	0.012	0.013	0.012	0.008	0.010	0.008	0.008	0.010	0.005	—	—
	B (9.6, 3.9, 0)	0.006	0.007	0.007	0.007	0.013	0.014	0.017	0.018	0.023	0.018	—	—
	t (3.9, 3.9, 3.9)	0.013	0.012	0.013	0.014	0.014	0.009	0.005	0.004	0.004	0.005	—	—
	T (9.6, 3.9, 3.9)	0.012	0.012	0.014	0.012	0.015	0.011	0.007	0.008	0.008	0.007	—	—
Y	n (0, 0, 0)	0.005	0.006	0.006	0.005	0.010	0.010	0.010	0.005	0.015	0.008	—	—
	u (3.9, 0, 0)	0.001	0.005	0.004	0.007	0.006	0.011	0.020	0.022	0.022	0.024	—	—
	U (9.6, 0, 0)	0.003	0.005	0.007	0.003	0.005	0.011	0.016	0.020	0.017	0.021	—	—
	b (3.9, 3.9, 0)	0.011	0.011	0.014	0.013	0.010	0.014	0.014	0.016	0.017	0.012	—	—
	B (9.6, 3.9, 0)	0.008	0.008	0.008	0.009	0.011	0.010	0.014	0.013	0.017	0.011	—	—
	t (3.9, 3.9, 3.9)	0.013	0.011	0.015	0.016	0.020	0.016	0.015	0.010	0.012	0.013	—	—
	T (9.6, 3.9, 3.9)	0.010	0.013	0.015	0.015	0.019	0.014	0.011	0.004	0.006	0.008	—	—
Z	n (0, 0, 0)	0.011	0.013	0.013	0.012	0.013	0.010	0.011	0.016	0.027	0.020	—	—
	u (3.9, 0, 0)	0.002	0.002	0.001	0.005	0.013	0.017	0.017	0.035	0.043	0.043	—	—
	U (9.6, 0, 0)	0.002	0.003	0.002	0.005	0.013	0.013	0.013	0.020	0.028	0.027	—	—
	b (3.9, 3.9, 0)	0.010	0.011	0.014	0.012	0.009	0.014	0.018	0.022	0.025	0.022	—	—
	B (9.6, 3.9, 0)	0.006	0.008	0.008	0.008	0.029	0.030	0.035	0.043	0.053	0.049	—	—
	t (3.9, 3.9, 3.9)	0.012	0.011	0.014	0.013	0.012	0.007	0.007	0.005	0.008	0.007	—	—
	T (9.6, 3.9, 3.9)	0.009	0.011	0.008	0.005	0.012	0.007	0.006	0.013	0.013	0.011	—	—

NOTES: